

Photoelectron momentum distributions of Ne and Xe dimers in counter-rotating circularly polarized laser fields

Zhi-Xian Lei(雷志仙), Qing-Yun Xu(徐清芸), Zhi-Jie Yang(杨志杰), Yong-Lin He(何永林), and Jing Guo(郭静)
Citation: Chin. Phys. B, 2022, 31 (**6**): 063202. DOI: 10.1088/1674-1056/ac4e05
Journal homepage: http://cpb.iphy.ac.cn; http://iopscience.iop.org/cpb

What follows is a list of articles you may be interested in

Molecular photoelectron momentum and angular distributions of N_2 molecules by ultrashort attosecond laser pulses

Si-Qi Zhang(张思琪), Qi Zhen(甄琪), Zhi-Jie Yang(杨志杰), Jun Zhang(张军), Ai-Hua Liu(刘爱华), Kai-Jun Yuan(元凯军), Xue-Shen Liu(刘学深), and Jing Guo(郭静)
Chin. Phys. B, 2021, 30 (**4**): 043201. DOI: 10.1088/1674-1056/abca22

Probing time delay of strong-field resonant above-threshold ionization

Shengliang Xu(徐胜亮), Qingbin Zhang(张庆斌), Cheng Ran(冉成), Xiang Huang(黄湘), Wei Cao(曹伟), and Peixiang Lu(陆培祥)
Chin. Phys. B, 2021, 30 (**1**): 013202. DOI: 10.1088/1674-1056/abc7a5

Ultrafast photoionization of ions and molecules by orthogonally polarized intense laser pulses: Effects of the time delay

Si-Qi Zhang(张思琪), Zhi-Jie Yang(杨志杰), Zhi-Xian Lei(雷志仙), Wei Feng(冯伟), Sheng-Peng Zhou(周胜鹏), Kai-Jun Yuan(元凯军), Xue-Shen Liu(刘学深), and Jing Guo(郭静)
Chin. Phys. B, 2021, 30 (**1**): 013201. DOI: 10.1088/1674-1056/abb30c

Tunable multistability and nonuniform phases in a dimerized two-dimensional Rydberg lattice

Han-Xiao Zhang(张焓笑), Chu-Hui Fan(范楚辉), Cui-Li Cui(崔淬砺), Jin-Hui Wu(吴金辉)
Chin. Phys. B, 2020, 29 (**1**): 013204. DOI: 10.1088/1674-1056/ab5d06

Origin of diffraction fringes in two-dimensional photoelectronmomentum distributions for single ionization of atoms in few-cycle intense laser pulses

Guo Zhi-Jian, Chen Zhang-Jin, Zhou Xiao-Xin
Chin. Phys. B, 2014, 23 (**4**): 043201. DOI: 10.1088/1674-1056/23/4/043201

Photoelectron momentum distributions of Ne and Xe dimers in counter-rotating circularly polarized laser fields

Zhi-Xian Lei(雷志仙), Qing-Yun Xu(徐清芸), Zhi-Jie Yang(杨志杰), Yong-Lin He(何永林), and Jing Guo(郭静)†

Institute of Atomic and Molecular Physics, Jilin University, Changchun 130012, *China*

(Received 22 November 2021; revised manuscript received 17 January 2022; accepted manuscript online 24 January 2022)

The strong-field ionization of dimers is investigated theoretically in counter-rotating circularly polarized laser fields. By numerically solving the two-dimensional (2D) time-dependent Schrödinger equation (TDSE) with the single-electron approximation (SEA) frame, we present the photoelectron momentum distributions (PMDs) and photoelectron angular distribution (PADs) of aligned Ne and Xe dimers. It is found that the PMDs and PADs strongly depend on the time delays by counter-rotating circularly polarized laser pulses. The results can be explained by the ultrafast photoionization model and the evolution of electron wave packets for Ne and Xe dimers. Besides, We make a comparison of PMDs between Ne atom and Ne dimer.

Keywords: time-dependent Schrödinger equation, dimer, photoelectron momentum distributions, ultrafast photoionization model

PACS: 32.80.Rm, 32.80.Fb, 42.50.Hz, 42.65.Re **DOI:** 10.1088/1674-1056/ac4e05

1. Introduction

Rapid developments in advanced laser technology provide new tools for investigating electron dynamics on its natural attosecond time scale (1 as = 10^{-18} s).[1–3] The interaction of laser pulses with atoms and molecules has become a hot topic in strong-field physics.[4] Ultrafast imaging of molecules with femtosecond temporal and sub-Angstrom spatial resolutions has emerged due to the development of x-ray free electron lasers.[5–11]

The ionization is one of the basic processes in strong-field physics. The ionized electron wave packets can produce various high-order nonlinear strong-field physical phenomena, such as multiphoton ionization,[12] above-threshold ionization,[13,14] high-order harmonic generation (HHG),[15,16] and nonsequential double ionization.[17,18] Observing the ionization dynamics of atoms and molecules under the intense laser fields and tracking them on the attosecond time scale can help us understand the motion of ionized electrons better. The photoelectron momentum distributions (PMDs) and photoelectron angular distributions (PADs) of atoms and molecules contain valuable information about the electron dynamics, which have attracted great attention of researchers over the past few years.[19–21] Besides, they are also important for detecting electron dynamics and the structure of atoms and molecules.

In recent years, the photoionization processes have been investigated in elliptically[22,23] and circularly polarized laser fields.[24,25] In 2016, Yuan *et al.*[21] theoretically explored the PMDs of hydrogen molecular ion by bichromatic circularly polarized pulses, which illustrates that the PMDs are sensitive to the molecular alignment and the parameters of the bichromatic co- and counter-rotating pulses. A pair of elliptically polarized laser pulses were used to investigate the role of initial states in photoelectron momentum distributions for Ne atom.[26] The interference effect of two emission centers for diatomic molecules on strong-field ionization (SFI) has attracted great attention, which has been suggested in 1966,[27] and then it was modeled in the photoionization of H_2 and H_2^+.[28] Nowadays it has been extended from perturbative regime to nonperturbative regime.[29] The influence of such interference effect on photoionization processes has been investigated for N_2, O_2, S_2, and F_2[30–33] with different initial states. The PMDs and PADs of N_2 and O_2 and their companion atoms (atoms with comparable ionization potentials) Ar and Xe, which were investigated experimentally and theoretically,[34] indicated that the influence of the parity of molecular HOMOs on the strong field molecular ionization dynamics. Recently, strong-field ionization (SFI) of the homonuclear noble gas dimer Ne_2[35] was investigated experimentally, which clearly showed an interference pattern in both circularly and linearly polarized laser fields and proved that two-center interference exists in Ne dimer. Then theoretical research[36] indicated the influence of double-slit interference on laser-induced dimer diffraction, and it also presented the dependence of the double-slit interference structure on the symmetry of the dimer orbitals and dimer orientation.

In the present work, we theoretically investigate the photoionization of Ne and Xe dimers by bichromatic ($\omega_1 = \omega_2$) counter-rotating circularly polarized laser fields with different time delays. The PMDs and PADs are dependent on the time delays, which derived from the interference between co-

†Corresponding author. E-mail: gjing@jlu.edu.cn

© 2022 Chinese Physical Society and IOP Publishing Ltd

herent electron wave packets emanating from the two nuclear centers. The ultrafast photoionization model[29] and the evolution of the electron wave packets are used to explain these results. Besides, we also compare the PMDs of Ne dimer with Ne atom and found that there are vortex patterns in the PMDs of Ne atom. The paper is arranged as follows: The theoretical model and computational methods are described in Section 2. The PMDs and PADs with different time delays of Ne and Xe dimers, and the differences between the PMDs of Ne dimer and Ne atom are presented and discussed in Section 3. Finally, we summarize our results in Section 4. Throughout this paper, atomic units (a.u.) $e = \hbar = m_e = 1$ are used unless otherwise stated.

2. Theoretical model and computational methods

We investigate the ionization of Ne and Xe dimers in counter-rotating circularly polarized laser pulses. As illustrated in Fig. 1(a), the Ne and Xe dimers are oriented in the (x,y) plane and are aligned along x axis. The two-dimensional (2D) time-dependent Schrödinger equation (TDSE) for dimers can be expressed as follows:

$$\mathrm{i}\frac{\partial \Psi(\boldsymbol{r},t)}{\partial t} = \left[\frac{\boldsymbol{p}^2}{2} + V(\boldsymbol{r}) + \boldsymbol{r}\cdot\boldsymbol{E}(t)\right]\Psi(\boldsymbol{r},t), \tag{1}$$

where $\boldsymbol{p}$ is the momentum of the electron, and $V(\boldsymbol{r})$ is the soft-core Coulomb potential of Ne and Xe dimers. The soft-core Coulomb potential of Ne dimer has the form[36]

$$V(\boldsymbol{r}) = -\sum_{\alpha=1}^{2}\frac{Z_\infty + (Z_0 - Z_\infty)\exp\left(-\dfrac{|\boldsymbol{r}-\boldsymbol{R}_\alpha|^2}{\sigma^2}\right)}{\sqrt{|\boldsymbol{r}-\boldsymbol{R}_\alpha|^2 + a^2}}. \tag{2}$$

Here $\boldsymbol{r} = (x,y)$ denotes the electron coordinate in x–y plane and α labels the nuclei located at fixed positions $\boldsymbol{R}_\alpha$. The effective nuclear charge Z_∞ and the bare charge Z_0 are 0.5 and 10, respectively. The soft-core parameter a is chosen to avoid singularity and σ is effective charge shielding parameter. The Ne dimer (Ne_2) has a ground-state molecular orbital configuration of $(1s\sigma_g)^2(1s\sigma_u)^2(2s\sigma_g)^2(2s\sigma_u)^2(2p\sigma_g)^2(2p\pi_u)^4(2p\pi_g)^4(2p\sigma_u)^2$. For the $2p\sigma_g$ orbital, $a = 1.200$ and $\sigma = 0.815$.[36] The internuclear distance $|R| = |R_1 - R_2| = 5.86$ a.u. for Ne_2, and the ionization potential of the ground state is $I_p = 0.747$ a.u.[37]

For Xe dimer, the molecular orbital configuration is $\cdots(5s\sigma_g)^2(5s\sigma_u)^2(5p\sigma_g)^2(5p\pi_u)^4(5p\pi_g)^4(5p\sigma_u)^2$,[38] and the soft-core Coulomb potential can be written as

$$V(\boldsymbol{r}) = -\sum_{\beta=1}^{2}\frac{Z_\beta(\boldsymbol{r}_\beta)}{\sqrt{|\boldsymbol{r}_\beta|^2 + 1}}, \tag{3}$$

where the analytical expression of $Z_\beta(\boldsymbol{r}_\beta)$ has the following form:

$$Z_\beta(\boldsymbol{r}_\beta) = 0.5 + (\rho_\beta - 0.5)\exp\left(-\frac{|\boldsymbol{r}_\beta|^2}{\sigma_\beta}\right), \tag{4}$$

$\boldsymbol{r}_\beta = \boldsymbol{r} - \boldsymbol{R}_\beta$ is the distance between the electron and the nucleus, $\boldsymbol{R}_\beta = \pm R_{(\mathrm{Xe-Xe})}/2$ is position of the nucleus and the internuclear distance is $R_{(\mathrm{Xe-Xe})} = 8.35$ a.u., $\rho_\beta = 9.2$, and $\sigma_\beta = 0.5$ are chosen to meet the ionization potential of the ground state, *i.e.*, $I_p = 0.44$ a.u.[38]

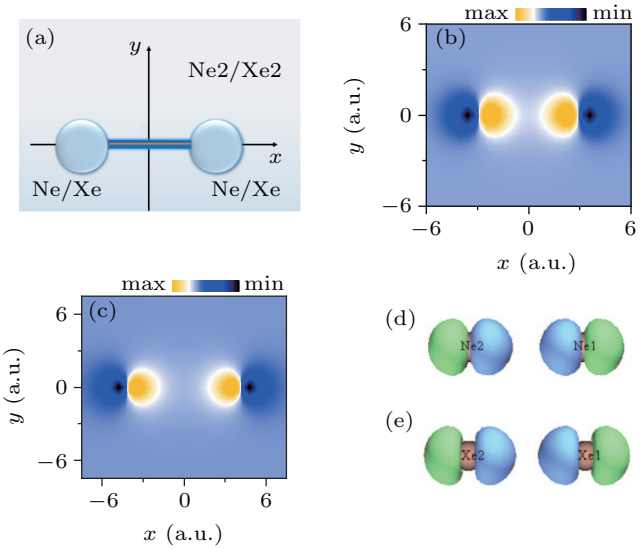


Fig. 1. (a) Ne and Xe dimers are oriented in the (x,y) plane, R is the distance between two nucleus. Panels (b) and (c) are the wave functions of $2p\sigma_g$ orbital for Ne dimer and $5p\sigma_g$ orbital for Xe dimer. Panels (d) and (e) are the wave functions of Ne dimer and Xe dimer obtained by GAUSSIAN09.

The interaction between dimers and the laser pulse is $V_L(\boldsymbol{r},t) = \boldsymbol{r}\cdot\boldsymbol{E}(t)$, $\boldsymbol{E}(t)$ is the electric field of counter-rotating circularly polarized pulses with time delay T_d, which can be expressed as

$$\boldsymbol{E}(t) = \boldsymbol{E}_1(t) + \boldsymbol{E}_2(t), \tag{5}$$

where

$$\boldsymbol{E}_1(t) = E_0 f(t)\left[\cos(\omega_1 t)\hat{e}_x + \sin(\omega_1 t)\hat{e}_y\right], \tag{6}$$

$$\boldsymbol{E}_2(t) = E_0 f(t+T_d)\{\cos[\omega_2(t+T_d)]\hat{e}_x - \sin[\omega_2(t+T_d)]\hat{e}_y\}, \tag{7}$$

where $E_0 = 0.107$ a.u. ($I_0 = 4\times10^{14}$ W/cm^2) is the amplitude of the electric fields. $\hat{e}_{x/y}$ is the laser polarization direction, $\omega_{1/2}$ ($\omega_1 = \omega_2$) is the angular frequency of laser fields, and the T_d is the time delay between two pulses. The pulse duration is $T = 20T_0$ ($T_0 = 2\pi/\omega_1$), and the pulse envelope $f(t) = \exp[-2(\ln 2)t^2/\tau^2]$ is used with $\tau = 2T_0$. In our calculation, the pulse duration is $T = 20T_0$ ($T_0 = 2\pi/\omega_1$), for Ne dimer $T \approx 44$ fs ($\omega_1 = 1.4$ a.u.) and for Xe dimer $T \approx 78$ fs ($\omega_1' = 0.78$ a.u.). According to supplemental material of Ref. [35], we can learn that for Ne dimer the time

required to reach an internuclear distance of 10 Å during direct dissociation starting at an internuclear distance of 3.1 Å is 600 fs–700 fs, while the indirect dissociation happens faster: an internuclear distance of 10 Å is reached within 200 fs–300 fs. Since the Xe and Ne are both noble gases, we believe that the time required for dissociation of Xe and Ne dimers are similar. Therefore, the dissociation for both dimers will not be taken into account in this paper.

The 2D TDSE can be solved by fast Fourier transform technique combined with split-operator method.[39,40] The imaginary-time propagation method has been used to obtain the initial wavefunction of Ne and Xe dimers. The wave functions for molecular ground state of Ne and Xe dimers are shown in Figs. 1(b) and 1(c). We can see that the two dimers are located along the molecular R axis with the σ_g symmetry. The ground state orbitals of Ne and Xe dimers are obtained by using the Hartree–Fock method with the $6-31+g$ (d,p) basis set as implemented in the GAUSSIAN09 program,[41] the results are shown in Figs. 1(d) and 1(e). Obviously they match the results obtained by the imaginary-time propagation method shown in Figs. 1(b) and 1(c), which also proves the correctness of our theoretical model.

The second-order split-operator method is used in our calculation to obtain the propagation of wave function,

$$\Psi(\boldsymbol{r},t+\Delta t) = \exp\left(-\mathrm{i}(\frac{p^2}{4})\Delta t\right)\exp\left(-\mathrm{i}\left[V(\boldsymbol{r})+V_{\mathrm{L}}(\boldsymbol{r},t)\right]\Delta t\right) \times \exp\left(-\mathrm{i}(\frac{p^2}{4})\Delta t\right)\Psi(\boldsymbol{r},t)+O(\Delta t)^3 \tag{8}$$

with time step $\Delta t = 0.05$ a.u., combined with fast Fourier transform (FFT) technique in spatial steps $\Delta x = \Delta y = 0.4$ a.u. In our calculation, the total spatial length is 409.6 a.u., which is large enough to prevent unphysical effects from the reflection of the wave packet from the boundary. At each time step, the wave function is multiplied by a mask function of the form $\cos^{(1/8)}$, and the domain of absorption ranges from $|x,y| = 150$ a.u. to $|x,y| = 204.8$ a.u. For the time-dependent electronic wave function $\Psi(\boldsymbol{r},t)$, the ionization part is recorded as $[1-M(\boldsymbol{r})]\Psi(\boldsymbol{r},t)$, and $\boldsymbol{r} = \sqrt{x^2+y^2}$,

$$M(\boldsymbol{r}) = \begin{cases} 1, & \boldsymbol{r} \le r_{\mathrm{b}}, \\ \exp\left[-\beta(\boldsymbol{r}-r_{\mathrm{b}})\right], & \boldsymbol{r} > r_{\mathrm{b}}, \end{cases} \tag{9}$$

where $\beta = 1$, and the boundary for ionized electron wave function and bounded wave function is set to be $r_{\mathrm{b}} = 80$ a.u. The photoelectron momentum distributions are acquired by Fourier transforming the ionized electron wave function into momentum space, the photoelectron angular distributions are obtained from the photoelectron momentum distributions.

3. Results and discussion

In the present work, the photoionization of Ne and Xe dimers by counter-rotating circularly polarized laser pulses with different time delays are illustrated. The PMDs and the PADs are presented in counter-rotating circularly polarized laser fields for Ne dimer at wavelengths $\lambda_1 = \lambda_2 = 32.5$ nm ($\omega_1 = \omega_2 = 1.4$ a.u.) and for Xe dimer at wavelengths $\lambda_1' = \lambda_2' = 58.5$ nm ($\omega_1' = \omega_2' = 0.78$ a.u.). Since the photon energy $\omega > I_{\mathrm{p}}$, the ionization process will occur by absorbing only one photon, which is called the single-photon process, where the Keldysh parameter $\gamma = \sqrt{I_{\mathrm{p}}/2U_{\mathrm{p}}} \gg 1$, the modification of the ionization potential by Stark shift can be ignored.

We firstly choose Ne dimer as a benchmark system to describe effects of the time delay T_{d} on PMDs and PADs in counter-rotating circularly polarized laser fields. In Fig. 2 we present the results calculated by TDSE simulations for $2p\sigma_{\mathrm{g}}$ orbital of Ne dimer in different time delays (0 o.c. [Figs. 2(a1) and 2(a2)], 2 o.c. [Figs. 2(b1) and 2(b2)], 4 o.c. [Figs. 2(c1) and 2(c2)], 6 o.c. [Figs. 2(d1) and 2(d2)]). The pulse wavelength, intensity and duration are respectively chosen as $\lambda_1 = \lambda_2 = 32.5$ nm ($\omega_1 = \omega_2 = 1.4$ a.u.), $E_0 = 0.107$ a.u. ($I_0 = 4\times 10^{14}$ W/cm^2) and $T = 20T_0$ ($T_0 = 2\pi/\omega_1$) with $\tau = 2T_0 = 2$ o.c. According to the energy conservation, with the laser pulse at wavelength $\lambda_1 = \lambda_2 = 32.5$ nm ($\omega_1 = \omega_2 = 1.4$ a.u.), the corresponding momentum is $P_{\mathrm{Ne2}} = \sqrt{2(\omega - I_{\mathrm{p}})} = 1.1$ a.u. One can see from Figs. 2(a1)–2(d1) that the PMDs of Ne dimer by counter-rotating circularly polarized laser pulses mainly have four components, and the strongest intensity of four components are localized at angles 70°, 110°, 250°, 290°. We can see that since the nucleus located at $(-R/2,0)$ and $(R/2,0)$ will attract electrons along the x-direction. As a result, it is easier for electrons to move along the y direction. Therefore, the electrons move farther along p_y than p_x. The PADs have six components from Figs. 2(a2)–2(d2), four radiation peaks with large amplitudes are located at angles 70°, 110°, 250°, 290°, and two radiation peaks with small amplitudes located at angles 0° and 180° can be ignored, which reflects the interference dynamics of molecular two-center photoionization processes in single-photon transition ($\omega > I_{\mathrm{p}}$). In Fig. 2(a2), at the time delay $T_{\mathrm{d}} = 0$ o.c., the PADs are mainly localized at ($\mathrm{P_{Ne2}} = 1.1$ a.u.) angles of 70°, 110°, 250°, 290° with almost equal intensity. At $T_{\mathrm{d}} = 2$ o.c. [Fig. 2(c2)], the distribution in the first and third quadrants becomes weaker. As the time delay increases, at $T_{\mathrm{d}} = 4$ o.c. [Fig. 2(c2)], the distribution becomes broader in the first and third quadrants and weaker in the second and fourth quadrants. When $T_{\mathrm{d}} = 6$ o.c. [Fig. 2(d2)], the distribution located in the first and third quadrants is much stronger than that in the second and fourth quadrants. It shows that the PMDs and PADs for Ne dimer are sensitive to the time delay.

The results can be explained by the ultrafast photoionization model of molecules[29,42] which has been successfully used to explain the two-center ionization process of hydrogen

molecular ion. For single-photon ionization process, the transition matrix element can be written as

$$W^{(1)} = \langle \Psi_c | \boldsymbol{D} \cdot \boldsymbol{E}_1(\varepsilon) | \Psi_0 \rangle e^{-i\eta_1}, \tag{10}$$

$$W^{(2)} = \langle \Psi_c | \boldsymbol{D} \cdot \boldsymbol{E}_2(\varepsilon) | \Psi_0 \rangle e^{-i\eta_2} \tag{11}$$

by counter-rotating circularly polarized laser pulses. $|\Psi_0\rangle$ and $|\Psi_c\rangle$ are the initial state and the continuum state respectively; $\boldsymbol{E}_1(\varepsilon) = \boldsymbol{e}_1 E_1(\varepsilon)$ and $\boldsymbol{E}_2(\varepsilon) = \boldsymbol{e}_2 E_2(\varepsilon)$ represent the Fourier transform of $\boldsymbol{E}_1(t)$ and $\boldsymbol{E}_2(t)$; $\boldsymbol{D} = \boldsymbol{n}D$ is the electric dipole operator, $\boldsymbol{n}$ is its unit vector direction; $\eta_1 = \phi_1$ is the phase of $\boldsymbol{E}_1(t)$ and $\eta_2 = \phi_2 + \omega_2 T_d$ is the phase of $\boldsymbol{E}_2(t)$. Therefore, the equations (10) and (11) can also be expressed as

$$W^{(1)} = \langle \Psi_c | D E_1(\varepsilon) | \Psi_0 \rangle (\boldsymbol{n} \cdot \boldsymbol{e}_1) e^{-i\eta_1}, \tag{12}$$

$$W^{(2)} = \langle \Psi_c | D E_2(\varepsilon) | \Psi_0 \rangle (\boldsymbol{n} \cdot \boldsymbol{e}_2) e^{-i\eta_2}. \tag{13}$$

To simplify the expression, we take $\sigma^1 = \langle \Psi_c | D E_1(\varepsilon) | \Psi_0 \rangle$ and $f^1 = (\boldsymbol{n} \cdot \boldsymbol{e}_1) e^{-i\eta_1}$, then $W^{(1)} = \sigma^1 f^1$. Likewise, $W^{(2)} = \sigma^2 f^2$, where $\sigma^2 = \langle \Psi_c | D E_2(\varepsilon) | \Psi_0 \rangle$ and $f^2 = (\boldsymbol{n} \cdot \boldsymbol{e}_2) e^{-i\eta_2}$. With counter-rotating circularly polarized laser pulses, the scalar product can be written as[21]

$$\boldsymbol{n} \cdot \boldsymbol{e}_1 = (\boldsymbol{n} \cdot \boldsymbol{e}_2)^* = \cos\theta + i \sin\theta, \tag{14}$$

where θ is the ejection angle, *i.e.*, the angle between the transition dipole momentum and the x axis. The total distribution reads

$$W = \left| W^{(1)} \right|^2 + \left| W^{(2)} \right|^2 + W^{(1,2)}, \tag{15}$$

where the interference term can be written as

$$W^{(1,2)} = W^{(1)*} W^{(2)} + W^{(1)} W^{(2)*} = \sigma^1 \sigma^2 f^{(1,2)}. \tag{16}$$

According to ultrafast photoionization model of molecules, the wave function in momentum space right after the laser pulse $\boldsymbol{E}(t) = \boldsymbol{E}\delta(t=0)$ is given by

$$\Psi(\boldsymbol{p}, 0^+) = \Psi(\boldsymbol{p} + \boldsymbol{A}), \tag{17}$$

where $\Psi(\boldsymbol{p}, 0^+)$ is the wavefunction of the initial state in the momentum $\boldsymbol{p}$ space, and $\boldsymbol{A}$ is the vector potential of the laser field. The wavefunction in coordinate space can be obtained by a Fourier transform of the function $\Psi(\boldsymbol{p}, 0^+)$, which is given by

$$\begin{aligned} \Psi(\boldsymbol{r}, 0^+) &= (2\pi)^{(-3/2)} \int e^{-i\boldsymbol{p}\cdot\boldsymbol{r}} \Psi(\boldsymbol{p}, 0^+) d\boldsymbol{p} \\ &= e^{-i\boldsymbol{A}\cdot\boldsymbol{r}} \Psi_0(\boldsymbol{r}), \end{aligned} \tag{18}$$

where $\Psi_0(\boldsymbol{r})$ is the initial wavefunction in coordinate space. Then transition amplitude can be written as

$$\begin{aligned} A(\boldsymbol{p}) &= (2\pi)^{(-3/2)} \int e^{-i\boldsymbol{p}\cdot\boldsymbol{r}} \Psi(\boldsymbol{r}, 0^+) d\boldsymbol{r} \\ &= (2\pi)^{(-3/2)} \int e^{-i\boldsymbol{p}\cdot\boldsymbol{r}} e^{-i\boldsymbol{A}\cdot\boldsymbol{r}} \Psi_0(\boldsymbol{r}) d\boldsymbol{r}. \end{aligned} \tag{19}$$

The ground state of Ne dimer is of gerade parity, the wavefunction of $2p\sigma_g$ is given by $\Psi_{2p\sigma_g}(\boldsymbol{r}) = (1/\sqrt{2})[\Psi_{2p}(\boldsymbol{r} - \boldsymbol{R}_{(Ne-Ne)}/2) - \Psi_{2p}(\boldsymbol{r} + \boldsymbol{R}_{(Ne-Ne)}/2)]$, which is a linear combination of 2p atomic orbital that are located at $\pm R_{(Ne-Ne)}/2$. By taking ultrafast photoionization model into account, the transition amplitude can thus be rewritten as

$$W^{(1)} \propto \sin[(\boldsymbol{p} + \boldsymbol{A}) \cdot \boldsymbol{R}/2] f^1, \tag{20}$$

$$W^{(2)} \propto \sin[(\boldsymbol{p} + \boldsymbol{A}) \cdot \boldsymbol{R}/2] f^2. \tag{21}$$

Since $U_p = (E_0^2/4\omega^2) \ll I_p$ and $\boldsymbol{A} \ll \boldsymbol{p}$, the vector potential of the laser field $\boldsymbol{A}$ in Eqs. (20) and (21) can be ignored to describe the photoionization processes. Then the interference term can be written as

$$\begin{aligned} W^{(1,2)} &= W^{(1)*} W^{(2)} + W^{(1)} W^{(2)*} \\ &\propto \sin^2(\boldsymbol{p} \cdot \boldsymbol{R}/2) \cos(2\theta + \Delta\eta), \end{aligned} \tag{22}$$

where $\Delta\eta = \eta_1 - \eta_2 = \omega_2 T_d$, and the equation (22) can be expressed as

$$W^{(1,2)} \propto \sin^2[pR\cos(\theta)/2] \cos(2\theta + \omega_2 T_d). \tag{23}$$

The term of cosine triangle functions $\cos(2\theta + \omega_2 T_d)$ presents the interference effects of the coherent electron wave packets due to the time delay of counter-rotating circularly polarized laser pulses, $\sin^2[(pR\cos(\theta))/2]$ presents the interference effects of the coherent electron wave packets emanating from the two nuclear centers. The results obtained from Eq. (23) are presented in Figs. 3(a)–3(d). By comparing Figs. 2 and 3, we can see that the angles of the radiation peaks of the PADs obtained from TDSE simulations in Fig. 2 are consistent with those predicted by the ultrafast ionization model in Fig. 3. However, the intensity of predicted results for PMDs in Fig. 3 cannot match the simulated results in Fig. 2 very well. The reason is as follows: the ultrafast ionization model is an oversimplified two-center model and the effects of the molecular Coulomb potential are not taken into account in the model,[43] which results in the intensity of predicted results for PADs cannot agree well with the simulated results.

In order to describe the intensity of the PMDs for Ne dimer, we display the evolution of the electron wave packets with time by counter-rotating circularly polarized laser pulses with different time delays in Fig. 4. The evolution of electron wave packet clearly shows the movement of electrons. At $t = 7.5$ o.c. [Figs. 4(a1)–4(d1)], the electrons are not ionized and the electrons are distributed around the nucleus. When $t = 12.34$ o.c. [Figs. 4(a2)–4(d2)], the electrons have been mainly ionized in four quadrants. When $t = 17.18$ o.c. [Figs. 4(a3)–4(d3)], there are more electron wave packets distributed in the range from 55° to 80°, from 100° to 125°, from 235° to 260° and from 280° to 305°, which are in agreement with the TDSE simulated results in Fig. 2. Meanwhile, we can see that at $t = 17.18$ o.c., *i.e.*, near the end of laser pulses, the

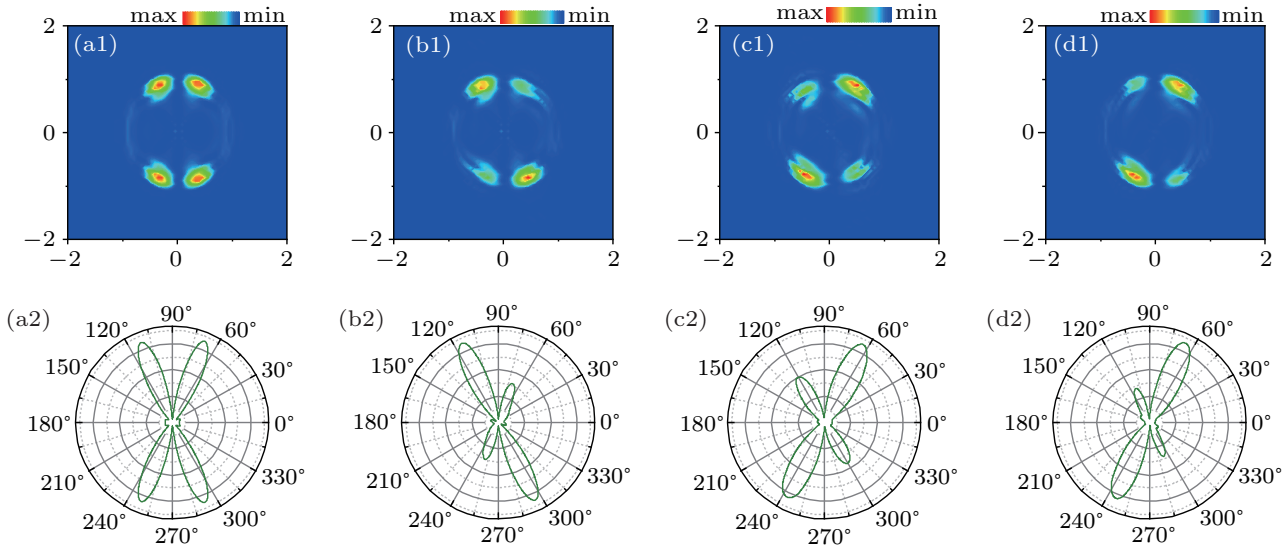


Fig. 2. PMDs and PADs of aligned Ne dimer at equilibrium internuclear distance $R_{(\mathrm{Ne-Ne})} = 5.86$ a.u. by counter-rotating circularly polarized laser pulses at $\lambda_1 = \lambda_2 = 32.5$ nm ($\omega_1 = \omega_2 = 1.4$ a.u.). The intensity of the laser pulses is $I_0 = 4 \times 10^{14}$ W/cm^2 ($E_0 = 0.107$ a.u.) and duration is $T = 20T_0$ ($T_0 = 2\pi/\omega_1$) with $\tau = 2T_0 = 2$ o.c. The upper row is the PMDs: (a1) $T_\mathrm{d} = 0$ o.c., (b1) $T_\mathrm{d} = 2$ o.c., (c1) $T_\mathrm{d} = 4$ o.c., (d1) $T_\mathrm{d} = 6$ o.c. The lower row is the PADs: (a2) $T_\mathrm{d} = 0$ o.c., (b2) $T_\mathrm{d} = 2$ o.c., (c2) $T_\mathrm{d} = 4$ o.c., (d2) $T_\mathrm{d} = 6$ o.c. The unit o.c. is short for optical cycle.

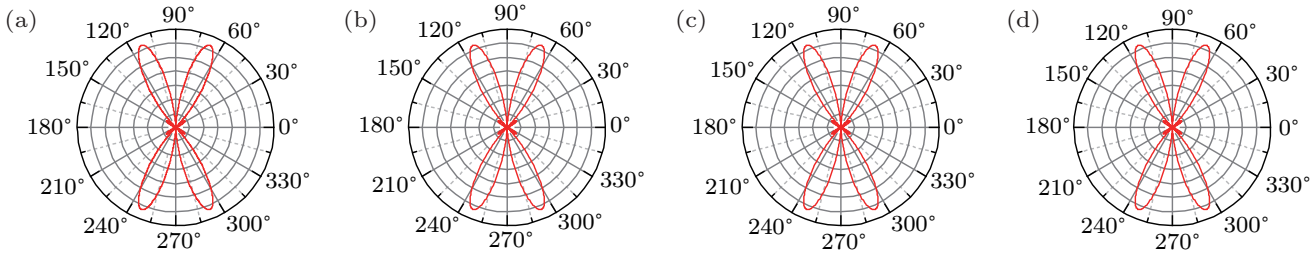


Fig. 3. The predicted results of PADs obtained from Eq. (23): (a) $T_\mathrm{d} = 0$ o.c., (b) $T_\mathrm{d} = 2$ o.c., (c) $T_\mathrm{d} = 4$ o.c., (d) $T_\mathrm{d} = 6$ o.c.

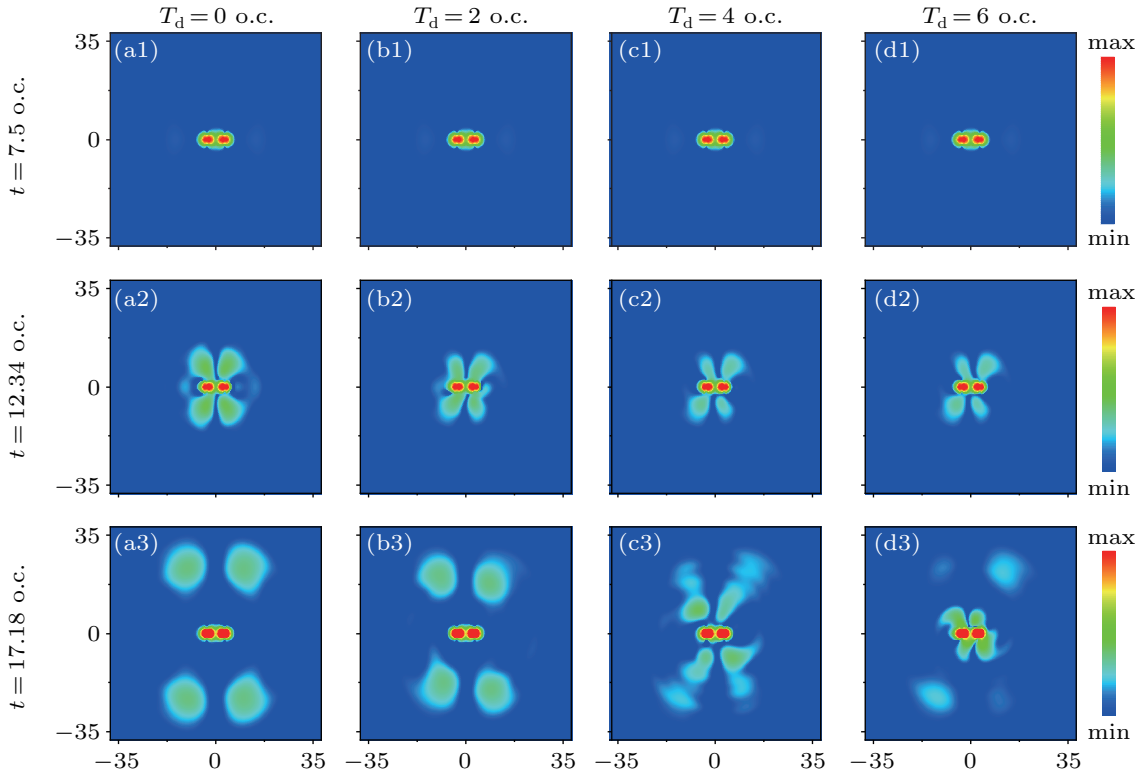


Fig. 4. The electron wave packets for the Ne dimer at different times by counter-rotating circularly polarized laser pulses at wavelength $\lambda_1 = \lambda_2 = 32.5$ nm ($\omega_1 = \omega_2 = 1.4$ a.u.) with four time delays: [(a1)–(a3)] $T_\mathrm{d} = 0$ o.c., [(b1)–(b3)] $T_\mathrm{d} = 2$ o.c., [(c1)–(c3)] $T_\mathrm{d} = 4$ o.c., and [(d1)–(d3)] $T_\mathrm{d} = 6$ o.c. The results are shown at three different times: [(a1)–(d1)] $t = 7.5$ o.c., [(a2)–(d2)] $t = 12.34$ o.c., and [(a3)–(d3)] $t = 17.18$ o.c.

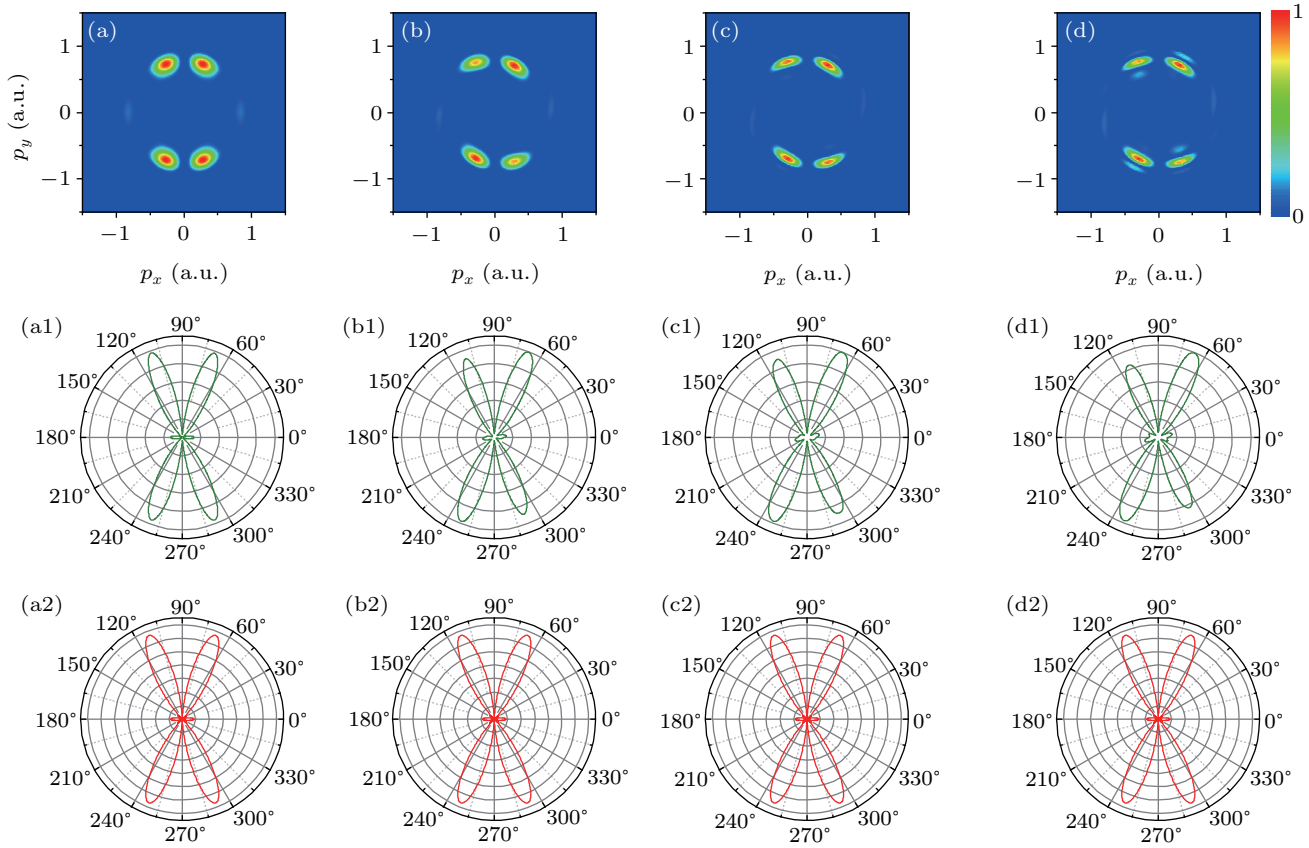


Fig. 5. The PMDs and PADs of aligned Xe dimer at equilibrium $R_{(\mathrm{Xe-Xe})} = 8.35$ a.u. by counter-rotating circularly polarized pulses at $\lambda_1' = \lambda_2' = 58.5$ nm ($\omega_1' = \omega_2' = 0.78$ a.u.). The intensity of the laser pulses is $I_0 = 4\times10^{14}$ W/cm^2 ($E_0 = 0.107$ a.u.) and duration is $T = 20T_0$ ($T_0 = 2\pi/\omega_1'$) with $\tau = 2T_0 = 2$ o.c. The PMDs and PADs simulated by TDSE are shown respectively for different time delays: (a) and (a1) $T_\mathrm{d} = 0$ o.c., (b) and (b1) $T_\mathrm{d} = 2$ o.c., (c) and (c1) T_d = 4 o.c., (d) and (d1) T_d = 6 o.c., The predicted results obtained from Eq. (26) are shown in: (a2) $T_\mathrm{d} = 0$ o.c., (b2) $T_\mathrm{d} = 2$ o.c., (c2) $T_\mathrm{d} = 4$ o.c., (d2) $T_\mathrm{d} = 6$ o.c.

images of electron wave packets are similar to the results of the final photoelectron momentum distributions (Fig. 2). For the time delay $T_\mathrm{d} = 0$ o.c. [Fig. 4(a3)], the electron wave packets are located in four quadrants with same intensity. For the time delay $T_\mathrm{d} = 2$ o.c. [Fig. 4(b3)], the electron wave packets are mainly located in the second and fourth quadrants rather than the first and third quadrants. When the time delay is 4 o.c. [Fig. 4(c3)], we find that the electron wave packets distributed in the first and third quadrants are enhanced while the distributions in the second and fourth quadrants become weaker. When the time delay is 6 o.c. [Fig. 4(d3)] the electron wave packets distributed in the first and third quadrants are much stronger than that in the second and fourth quadrants. The results for the evolution of electron wave packets are in full agreement with the results of the PMDs in Fig. 2.

Similarly, We choose Xe dimer to investigate effects of the time delay T_d on photoelectron momentum distributions by counter-rotating circularly polarized laser pulses. The wavelength, intensity and duration are respectively chosen as $\lambda_1' = \lambda_2' = 58.5$ nm ($\omega_1' = \omega_2' = 0.78$ a.u.), $E_0 = 0.107$ a.u. ($I_0 = 4\times10^{14}$ W/cm^2) and $T = 20T_0$ ($T_0 = 2\pi/\omega_1'$) with $\tau = 2T_0 = 2$ o.c. We present the photoelectron angular distributions (PADs) obtained by TDSE simulations of Xe dimer in different time delays (0 o.c. [Fig. 5(a)], 2 o.c. [Fig. 5(b)], 4 o.c. [Fig. 5(c)], 6 o.c. [Fig. 5(d)]). According to the energy conservation, with the laser pulse at wavelength $\lambda_1' = \lambda_2' = 58.5$ nm ($\omega_1' = \omega_2' = 0.78$ a.u.) the corresponding momentum is $P_{\mathrm{Xe}_2} = \sqrt{2(\omega - I_\mathrm{p})} = 0.825$ a.u. From Figs. 5(a1)–5(d1), the PADs of Xe dimer mainly have four components, and the peak intensity of four components are localized at angles 70°, 110°, 250°, 290°, the angle distributions are almost the same as the results of Ne dimer. In Fig. 5(a1), at time delay $T_\mathrm{d} = 0$ o.c., the intensity of PMDs is the same in four quadrants. While as the time delay increases, the intensity of PMDs in the second and fourth quadrants become weaker. At $T_\mathrm{d} = 6$ o.c., the intensity of PMDs in the first and third quadrants is much stronger than that in the second and fourth quadrants. Comparing the PADs of Ne dimer (Figs. 2(a2)–2(d2)) and Xe dimer (Figs. 5(a1)–5(d1)), for the first and third quadrants, the intensity distributions of Ne dimer is weakened first and then enhanced while that of Xe dimer are almost unchanged. The same is, for the second and fourth quadrants, the intensity distributions of both Ne dimer and Xe dimer become weaker and weaker with increasing time delay.

We also describe the photoionization process by the ultrafast photoionization model, the derivation process of Xe dimer is the same as the Eqs. (10)–(19) for Ne dimer, the initial state of Xe dimer is of gerade parity, the wavefunction is

given by $\Psi_{5p\sigma_g}(\boldsymbol{r}) = (1/\sqrt{2})[\Psi_{5p}(\boldsymbol{r} - \boldsymbol{R}_{(\mathrm{Xe-Xe})}/2) - \Psi_{5p}(\boldsymbol{r} + \boldsymbol{R}_{(\mathrm{Xe-Xe})}/2)]$, which is a linear combination of $5p$ atomic orbital that are located at $\pm R_{(\mathrm{Xe-Xe})}/2$. By taking ultrafast photoionization model into account, the transition amplitude can thus be rewritten as

$$W^{(1)} \propto \sin[(\boldsymbol{p} + \boldsymbol{A}) \cdot \boldsymbol{R}/2] f^1, \tag{24}$$

$$W^{(2)} \propto \sin[(\boldsymbol{p} + \boldsymbol{A}) \cdot \boldsymbol{R}/2] f^2. \tag{25}$$

Then the interference term can be written as

$$W^{(1,2)} \propto \sin^2(PR\cos(\theta)/2)\cos(2\theta + \omega_2 T_\mathrm{d}). \tag{26}$$

The corresponding predicted results obtained from Eq. (26) are presented in Figs. 5(a2)–5(d2). Comparing Figs. 5(a1)–5(d1) with Figs. 5(a2)–5(d2), we can see that the same angle distributions are presented, but the amplitude of PMDs predicted cannot agree well with the results of TDSE sumilations. Similarly, we present the amplitude of PMDs simulated by TDSE for Xe dimer by the evolution of the electron wave packets in counter-rotating circularly polarized laser fields with different time delays in Fig. 6.

In Figs. 6(a1)–6(a3), when $T_\mathrm{d} = 0$ o.c., from $t = 7.5$ o.c. to $t = 17.18$ o.c., we can see that the electron wave packets are located in four quadrants with same intensity, which agrees well with the TDSE simulation results in Fig. 5(a1). When $T_\mathrm{d} = 2$ o.c., 4 o.c., and 6 o.c., the electrons are ionized along four quadrants and are mainly distributed in the first and third quadrants over time as shown in Figs. 6(b1)–6(b3), 6(c1)–6(c3), and 6(d1)–6(d3). At $t = 17.18$ o.c., there are more electrons distributed in the first and third quadrants than that in the second and fourth quadrants, which corresponds with the TDSE results in Figs. 5(b1)–5(d1). Therefore, the evolution of electron wave packets also can be used to explain the amplitudes of PMDs for Xe dimer successfully.

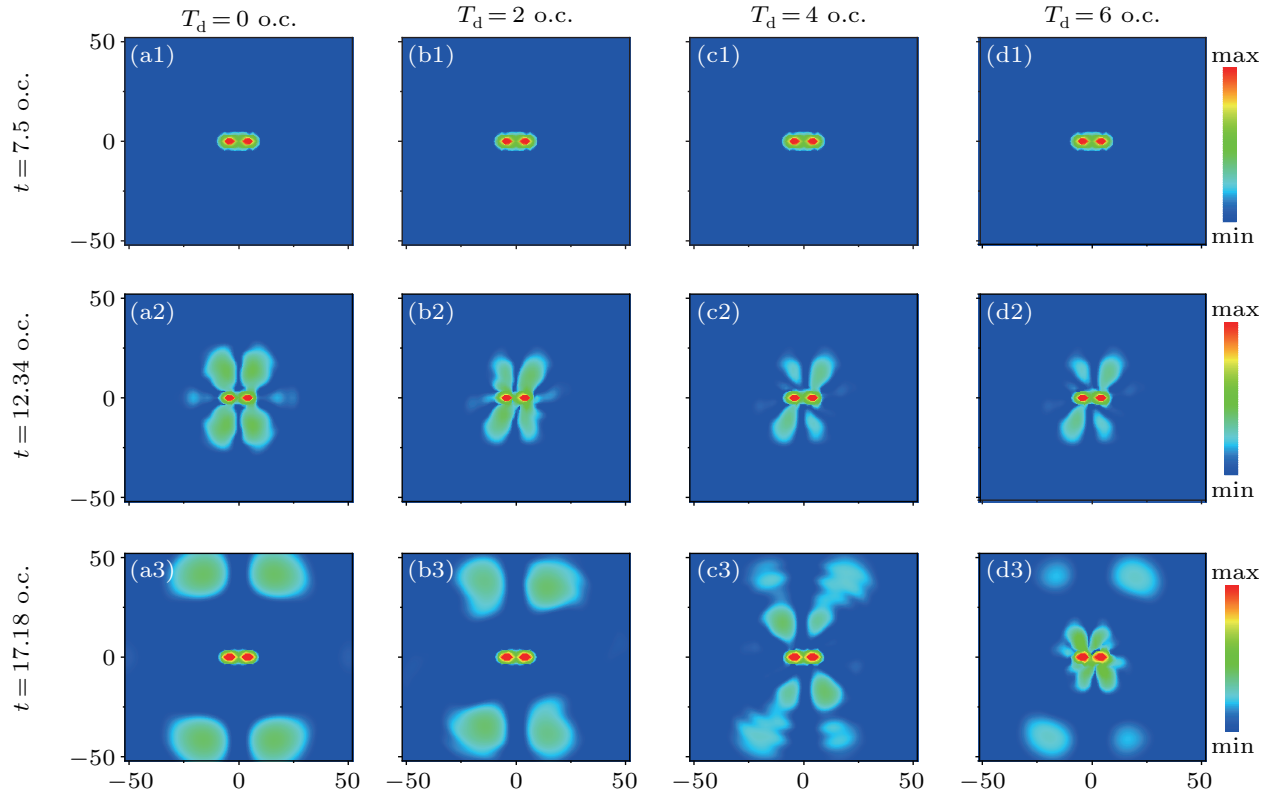


Fig. 6. The electron wave packets for the Xe dimer at different times by counter-rotating circularly polarized laser pulses at wavelength $\lambda_1' = \lambda_2' = 58.5$ nm ($\omega_1' = \omega_2' = 0.78$ a.u.) with four time delays: [(a1)–(a3)] $T_\mathrm{d} = 0$ o.c., [(b1)–(b3)] $T_\mathrm{d} = 2$ o.c., [(c1)–(c3)] $T_\mathrm{d} = 4$ o.c., and [(d1)–(d3)] $T_\mathrm{d} = 6$ o.c. The results are shown at three different times: [(a1)–(d1)] $t = 7.5$ o.c., [(a2)–(d2)] $t = 12.34$ o.c., and [(a3)–(d3)] $t = 17.18$ o.c.

To compare the photoionization of Ne dimer and Ne atom, we investigate the photoionization of $2p_-$ excited state of Ne atom with magnetic quantum number $m = -1$ by time-delayed counter-rotating circularly polarized laser pulses. Figures 7(a)–7(d) display the PMDs of Ne atom with different time delays for the $2p_-$ state ($I_{2p_-} = 0.793$ a.u.) as the initial electronic state.

Figures 7(a)–7(d) show that the PMDs of Ne atom present two spiral arms at wavelength $\lambda_1 = \lambda_2 = 20$ nm ($\omega_1 = \omega_2 = 2.28$ a.u.), and we can see that the PMDs are also sensitive to the time delay. The physical mechanism of electron vortices generation is the coherent superposition of photoelectron wave packets with time delay and different magnetic quantum number m. The valence electron in $2p_-$ state can be ionized via following route by absorbing one photon from the first left-handed circularly polarized laser pulse (E_1) ($|p,-1\rangle \rightarrow |d,0\rangle$)

or the second right-handed circularly polarized laser pulse (E_2) ($|p,-1\rangle \rightarrow |d,-2\rangle$), as shown in Fig. 8. Owing to time delay between the two pulses, a phase of $e^{-iE'T_d/\hbar}$ will be generated in the final electron wavepacket by the first pulse, in which E' represents the photoelectron energy.[44] The final superposition state reads

$$|\Psi_2\rangle \propto e^{-iE'T_d/\hbar}|d,0\rangle + |d,-2\rangle . \tag{27}$$

The interference of $|d,0\rangle$ and $|d,-2\rangle$ states generates a vortex pattern with C_2 rotational symmetry as shown in the Figs. 7(a)–7(d), and with the increasing time delay, the spiral arms become longer and thinner, which consists with the results in Ref. [45].

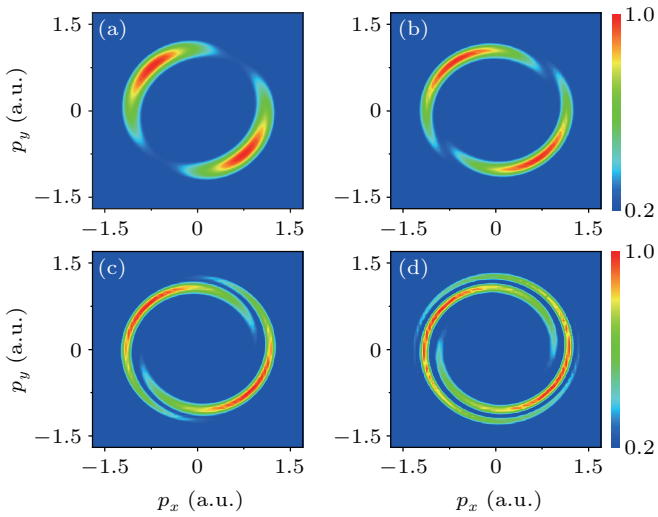


Fig. 7. PMDs of Ne atom by counter-rotating circularly polarized laser pulses with time delay T_d at $\lambda_1 = \lambda_2 = 32.5$ nm ($\omega_1 = \omega_2 = 1.4$ a.u.). The intensity of the laser pulses is $I_0 = 4\times10^{14}$ W/cm^2 ($E_0 = 0.107$ a.u.) and duration is $T = 20T_0$ ($T_0 = 2\pi/\omega_1$) with $\tau = 2T_0 = 2$ o.c., which are the same parameters as Ne dimer. Results are shown for four time delays: (a) $T_d = 0$ o.c., (b) $T_d = 2$ o.c., (c) $T_d = 4$ o.c., and (d) $T_d = 6$ o.c.

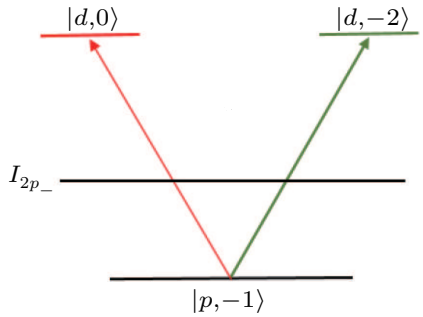


Fig. 8. Single-photon ionization channel scheme for photoionization of Ne atom with the initial electronic state of $2p_-$ by counter-rotating circularly polarized laser pulses.

The results of PMDs of Ne atom are obviously different from that of Ne dimer. We consider that the initial structure of Ne dimer maybe the reason of the absence of vortex patterns in its PMDs. Furthermore, the highly symmetry of the initial state of Ne atom may be an important reason for the appearance of the vortex patterns.

4. Conclusion

The photoionization of molecular ground state of Ne dimer and Xe dimer in counter-rotating circularly polarized laser fields are investigated theoretically. Simulations are performed on the Ne and Xe dimers by numerically solving corresponding 2D TDSEs. Our numerical results show the PMDs and PADs of Ne and Xe dimers are dependent on the time delays, which comes from the interference between coherent electron wave packets created by the time delay of two counter-rotating circularly polarized laser pulses. The ultrafast photoionization model and the evolution of the electron wave packets are adopted to well explain the results. In the comparison between Ne dimer and Ne atom, We found that the PMDs of Ne atom present vortex patterns. And we believe that the disappearance of the vortex patterns for Ne dimer can be attributed to the structure of initial state for Ne dimer.

Acknowledgment

Project supported by the National Natural Science Foundation of China (Grant No. 12074146).

References

[1] Brabec T and Krausz F 2000 *Rev. Mod. Phys.* **72** 545
[2] Xiao F, Fan X H, Wang L, Zhang D W, Wu J H, Wang X W and Zhao Z X 2020 *Chin. Phys. Lett.* **37** 114202
[3] Wang X W, Wang L, Xiao F, Zhang D W, Lü Z H, Yuan J M and Zhao Z X 2020 *Chin. Phys. Lett.* **37** 023201
[4] Mourou G A, Labaune C L, Dunne M, Naumova N and Tikhonchuk V T 2007 *Plasma Phys. Control. Fusion* **49** B667
[5] Emma P, Akre R, Arthur J *et al.* 2010 *Nat. Photon.* **4** 641
[6] Ishikawa T, Aoyagi H, Asaka T *et al.* 2012 *Nat. Photon.* **6** 540
[7] Margaritondo G 2017 *Nuovo Cimento Rivista Serie* **40** 411
[8] Elsaesser T 2017 *Chem. Rev.* **117** 10621
[9] Elsaesser T and Woerner M 2014 *J. Chem. Phys.* **140** 020901
[10] Miller R J D 2016 *Faraday Discuss.* **194** 777
[11] Xu J L, Blaga C I, Agostini P and DiMauro L F 2016 *J. Phys. B: At. Mol. Opt. Phys.* **49** 112001
[12] Nakajima T 2009 *Phys. Rev. A* **79** 043414
[13] Agostini P, Fabre F, Mainfray G, Petite G and Rahman N K 1979 *Phys. Rev. Lett.* **42** 1127
[14] Li M, Geng J W, Liu H, Deng Y K, Wu C Y, Peng L Y, Gong Q H and Liu Y Q 2014 *Phys. Rev. Lett.* **112** 113002
[15] Miao X Y and Zhang C P 2014 *Laser Phys. Lett.* **11** 115301
[16] Chen Y J and Fu L B and Liu J 2013 *Phys. Rev. Lett.* **111** 073902
[17] Fittinghoff D N, Bolton P R, Chang B and Kulander K C 1992 *Phys. Rev. Lett.* **69** 2642
[18] Walker B, Sheehy B, DiMauro L F, Agostini P, Schafer K J and Kulander K C 1994 *Phys. Rev. Lett.* **73** 1227
[19] Ma M Y, Wang J P, Jing W Q, Guan Z, Jiao Z H, Wang G L, Chen J H and Zhao S F 2021 *Opt. Express* **29** 33245
[20] Tang J, Zhang G Z, He Y F, Li M, Ding X and Yao J Q 2020 *Chin. Phys. Lett.* **37** 024201
[21] Yuan K J, Chelkowski S and Bandrauk A D 2016 *Phys. Rev. A* **93** 053425
[22] Wang S, Cai J and Chen Y J 2017 *Phys. Rev. A* **96** 043413
[23] Tong A H, Zhou Y M and Lu P X 2017 *Opt. Quantum Electron.* **49** 77
[24] Djiokap J N, Hu S X, Madsen L B, Manakov N L, Meremianin A V and Starace A F 2015 *Phys. Rev. Lett.* **115** 113004
[25] Pham V N T, Tolstikhin O I and Morishita T 2019 *Phys. Rev. A* **99** 013428

[26] Cui H F and Miao X Y 2020 *Chin. Phys. B* **29** 074203
[27] Cohen H D and Fano U 1966 *Phys. Rev.* **150** 30
[28] Walter M and Briggs J 1999 *J. Phys. B: At. Mol. Opt. Phys.* **32** 2473
[29] Zuo T, Bandrauk A D and Corkum P B 1996 *Chemical Physics Letters* **259** 313
[30] Talebpour A, Chien C Y and Chin S L 1996 *J. Phys. B: At. Mol. Opt. Phys.* **29** L677
[31] Guo C, Li M, Nibarger J P and Gibson G N 1998 *Phys. Rev. A* **58** R4271
[32] Dewitt M J , Wells E and Jones R R 2001 *Phys. Rev. Lett.* **87** 153001
[33] Grasbon F, Paulus G G, Chin S L, Walther H, Muth-Böhm J, Becker A and Faisal F H M 2001 *Phys. Rev. A* **63** 041402
[34] Wei M Z, Quan W, Sun R P, Xu S P, Xiao Z L, Zhou Yu, Zhao M, Hao X L, Duan C X and Liu X J 2018 *Phys. Rev. A* **98** 063418
[35] Kunitski M, Eicke N, Huber P *et al.* 2019 *Nat. Commun.* **10** 1
[36] Guo Z N and Liu Y Q 2020 *J. Phys. B: At. Mol. Opt. Phys.* **53** 065004
[37] https://webbook.nist.gov/chemistry/
[38] Pradeep T, Niu B and Shirley D A 1993 *J. Chem. Phys.* **98** 5269
[39] Bandrauk A D and Shen H 1993 *J. Chem. Phys.* **99** 1185
[40] Bandrauk A D and Lu H Z 2013 *J. Theor. Comput. Chem.* **12** 1340001
[41] Frisch M, Trucks G, Schlegel H B, *et al.* 2009 *GAUSSIAN09* (Inc., Wallingford CT)
[42] Zhang H D, Ben S, Xu T T and Song K L 2018 *Phys. Rev. A* **98** 013422
[43] Yuan K J, Lu H Z and Bandrauk A D 2017 *J. Phys. B: At. Mol. Opt. Phys.* **50** 124004
[44] Pengel D, Kerbstadt S, Johannmeyer D, Englert L, Bayer T and Wollenhaupt M 2017 *Phys. Rev. Lett.* **118** 053003
[45] Guo J, Zhang S Q, Zhang J, Zhou S P and Guan P F 2021 *Laser Physics* **31** 065301